Journal of Power Sources 222 (2013) 282–287

Contents lists available at SciVerse ScienceDirect

Journal of Power Sources

journal homepage: www.elsevier.com/locate/jpowsour

Oxide ion diffusion in Ba-doped $LaInO_3$ perovskite: A molecular dynamics study

Dae-Seop Byeon [a,b], Seong-Min Jeong [a,*], Kuk-Jin Hwang [a,c], Mi-Young Yoon [c], Hae-Jin Hwang [c], Shin Kim [d], Hong-Lim Lee [b]

[a] Business Support Division, Korea Institute of Ceramic Engineering and Technology (KICET), 233-5 Gasan-dong, Geumcheon-gu, Seoul 153-801, Republic of Korea
[b] Department of Materials Science and Engineering, Yonsei University, Seoul 120-749, Republic of Korea
[c] School of Materials Science and Engineering, Inha University, Incheon 120-749, Republic of Korea
[d] Hasla Co. Ltd, Gangneung 210-340, Republic of Korea

HIGHLIGHTS

- The trajectories of ions were analyzed through molecular dynamics.
- The Ba dopant in the $LaInO_3$ forms bottlenecks with various sizes.
- Small bottlenecks were proved to block the migrations of oxygen ions.
- Oxygen conduction was affected by the distribution of doped Ba ions.

ARTICLE INFO

Article history:
Received 23 May 2012
Received in revised form
26 August 2012
Accepted 27 August 2012
Available online 10 September 2012

Keywords:
Diffusion pathway
Solid oxide fuel cell
Molecular dynamics
Oxide ion conductivity
Perovskite

ABSTRACT

A computational study employing classical molecular dynamics techniques was employed to explore the diffusion of oxide ions in Ba-doped $LaInO_3$, a cubic perovskite oxide. The Ba dopant in the $LaInO_3$ forms oxygen vacancies that function as charge carriers via an oxygen diffusion mechanism. Previous experimental studies reported that the ionic conductivity of Ba-doped $LaInO_3$ decreases with increasing numbers of oxygen vacancies, which was not fully understood through experimental approaches. Hence, this study explored the diffusion pathway for individual oxygen vacancies through molecular dynamics simulation. Based on the findings of this study, the Ba dopant appears to form narrow bottlenecks that function as a barrier to the movement of oxide ions. We concluded that the oxide ion conductivity of Ba-doped $LaInO_3$ is affected by the local ionic distribution of the Ba dopant.

1. Introduction

Ternary oxides with a ABO_3 perovskite structure shown in Fig. 1 can tolerate high concentrations of various dopants. Such dopants can alter the properties of the material, conferring a sufficiently high oxide ion conductivity that permits it to be applied to an electrolyte for solid oxide fuel cells (SOFC), electrolysers, oxygen pumps and amperometric oxygen monitors. Hence, for more than three decades, a number of research groups have attempted to enhance the oxide ion conductivity in these materials by replacing *A*- and/or *B*-site cations with acceptor species. It is well known that *A*-site cation doped $LaBO_3$ perovskites (B = Al, Ga, Sc, In and rare-earth ions) are oxide ion conductors, a property that has attracted considerable interest [1–6]. Among these materials, Ba-doped $LaInO_3$, $(Ba_xLa_{1-x})InO_{3-0.5x}$, has shown some interesting characteristics [5,6]. These materials exist as a single phase in the range from $x = 0.4$ to $x = 1$. The crystal symmetries of the single phases were found to be cubic in the composition range from $x = 0.4$ to $x = 0.5$, tetragonal from $x = 0.5$ to $x = 0.8$ and orthorhombic above $x = 0.8$ [5]. The highest ionic conductivity of this material was obtained in the region where the material exists as a cubic phase in the composition range from $x = 0.4$ to $x = 0.5$. This material shows the characteristics of both an oxygen-ion and a p-type conductor at high partial pressures of oxygen under a dry atmosphere, but behaves as a pure oxide ion conductor in a N_2 atmosphere [5,6]. At temperatures below 450 °C, it becomes a proton conductor in a wet atmosphere.

Although the conduction of protons in $(Ba_xLa_{1-x})InO_{3-0.5x}$ has been examined in previous studies [5,6], the mechanism for the oxygen-ion conduction of this material is not currently fully understood. Oxide ion conductivity is generally affected by

* Corresponding author. Tel.: +82 2 3282 7825; fax: +82 2 3282 2490.
E-mail address: smjeong@kicet.re.kr (S.-M. Jeong).

0378-7753/$ – see front matter © 2012 Elsevier B.V. All rights reserved.
http://dx.doi.org/10.1016/j.jpowsour.2012.08.091

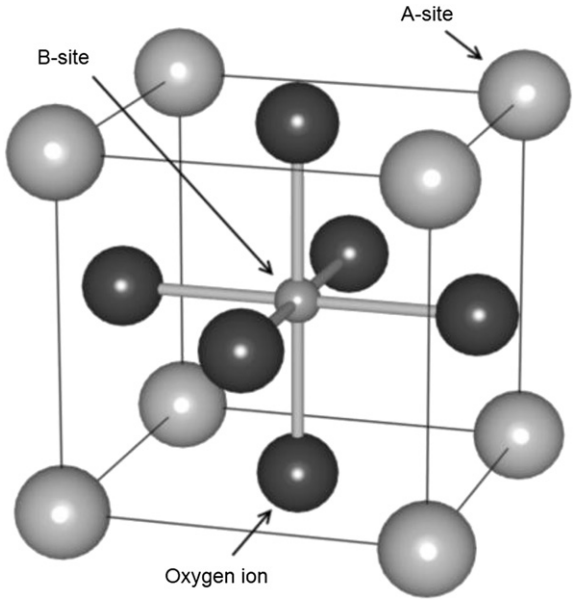

Fig. 1. Typical perovskite structure.

a multitude of complicating factors, including the unit cell free volume, the radius of the dopant ion used, the number of oxygen vacancies, and the crystal symmetry. For an example, the increase of oxygen vacancies usually enhances oxide ion conductivity. However, the ionic conductivity of $(Ba_xLa_{1-x})InO_{3-0.5x}$ decreases with increasing numbers of oxygen vacancies, which has been not been fully understood through pure experimental approaches [5,6].

Meanwhile, molecular dynamics simulations employing a vacancy diffusion model have been developed for analyzing such experimental results and have been applied to the study of the conductivity of oxygen by perovskite oxides [7–11]. Cherry et al. [7] and Islam et al. [8,9] investigated the migration of oxide ions $LaBO_3$(B = Cr, Mn, Fe, Co) and Sr doped $LaBO_3$(B = Mn, Co) perovskite oxides and successfully analyzed the oxide ion path, characterized as having a saddle point. Yamamura et al. proposed the use of materials design methodology based on a molecular dynamics simulation technique by replacing A- and B-site cations for perovskite based oxide ion conductors [10]. Fisher et al. studied the relationship between the conductivity of oxide ions and the dopant content for Sr-doped $BaBO_3$ (B = Co, Fe) [11].

Therefore, in this study, we explored the open question of oxide ion conduction in Ba-doped $LaInO_3$ perovskite by employing a molecular dynamics simulation with a vacancy diffusion model. We calculated both the trajectory of ions in the calculation box and the oxide ion conductivity, which provided us with a straight solution for understanding the conduction of oxide ions in Ba-doped $LaInO_3$. Various configurations of Ba-doped $LaInO_3$ perovskite were analyzed for the local distribution of A- and B-sites cations, which clearly revealed that the mechanism of oxide ion diffusion is clearly related to the local distributions of ions in such materials.

2. Simulation method

The interatomic potentials employed in this study consisted of a Coulombic term, a short range repulsion term and a dispersion term, which is known as the Born model framework [12–14] as follows:

$$U_{ij} = \frac{q_i q_j}{r_{ij}} + f_0(b_i + b_j)\,\exp\left[\frac{a_i + a_j - r_{ij}}{b_i + b_j}\right] - \frac{c_i c_j}{r_{ij}^6} \quad (1)$$

In eq. (1) the first term represents the long-range Coulombic or electrostatic interaction between each pair of ions i and j in the structure, r_{ij} is the distance between ions i and j, The second term of the interatomic potentials describes short-range repulsion, f_0 is a constant for unit adaptation (=1 kcal mol^{-1} Å^{-1}), q_i is the effective charge of ion i and a and b are parameters for each ion. The third term represents the dipole-induced dipole dispersion potential related to van der Waals interactions. All calculations were carried out using the MD simulation software LAMMPS (Sandia National Laboratory, USA) [15].

According to previous studies, $(Ba_xLa_{1-x})InO_{3-0.5x}$ has a cubic structure between $x = 0.4$ and $x = 0.8$. Hence, the amount of Ba dopant used for the calculation was in the range from 0.4 to 0.8, in incremental steps of 0.1. In all cases, La and In were assumed to be trivalent cations, while Ba and O were assumed to be a divalent cation and an anion respectively. This means that one O is removed by replacing two La cations with two Ba cations. All of the ions were applied to the calculation with 85% of the formal charge considering the effective ionic bonding fraction [10]. Table 1 shows the potential parameters for the La, Ba, In and O ions used in this study. The simulation model consisted of 200 ($8 \times 5 \times 5$) primitive cubic cells. Since some oxide ions were removed to maintain charge neutrality, the number of ions in the models range from 920 ($x = 0.8$) to 960 ($x = 0.4$). Since 200 primitive cells were modeled for the MD simulation and each cell contains 3 available oxygen sites, making the total number of oxygen sites to be 600. Each oxide ion forms an octahedron facing 8 adjacent oxygen octahedra. Therefore, the total number of available oxygen site pairs between adjacent oxygen octahedra is 2400 in this study.

Newton's equation of motion was integrated for 2 ns with a time step of 1 fs, after a relaxation stage for 2 ns to remove the effect of the initial arrangement of oxygen vacancies. Each model with various compositions was simulated at temperatures from 800 °C to 1200 °C under a pressure of 1 bar.

To derive the ionic conductivity, the mean square displacement (MSD) of oxide ion was calculated according to

$$\mathrm{MSD}(t) = \frac{1}{N}\sum_{i=0}^{N}(r(t) - r(0))^2 \quad (2)$$

where N is the total number of ions and $r(t)$ is the position of an ion i at the time t.

MSD has a relation to the diffusion coefficient as the Einstein relation

$$\mathrm{MSD}(t) = 6Dt \quad (3)$$

where t is the time and D the diffusion coefficient. The ionic conductivity was obtained from the diffusion coefficient according to the Nernst–Einstein equation

$$\sigma = \frac{q^2 ND}{fk_B TV} \quad (4)$$

where σ is ionic conductivity, k_B is Boltzmann constant, T is temperature, f is Haven ratio, V is volume and q is the ion's charge. f had been calculated 0.69 for the perovskite structure [17].

Table 1
Potential parameters of ions for $(Ba_xLa_{1-x})InO_{3-0.5x}$.

Ions	a (Å)	b (Å)	c (kcal Å^6 mol^{-1})	Ref.
La	2.1493	0.205	0	[10]
Ba	1.8000	0.077	0	[16]
In	2.0134	0.220	0	[10]
O	1.56775	0.0865	27	[10]

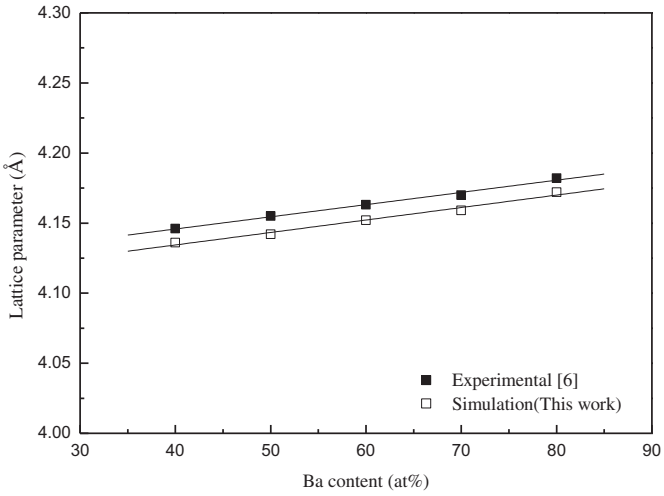

Fig. 2. Lattice parameters of $(Ba_xLa_{1-x})InO_{3-0.5x}$ as a function of Ba content compared with experimental values.

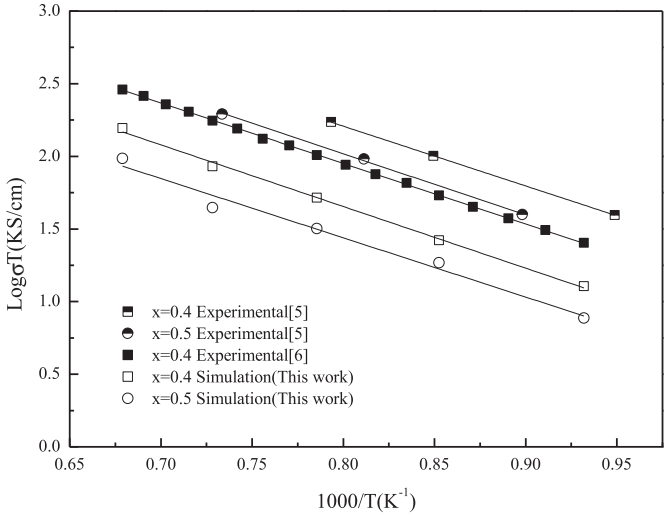

Fig. 4. Arrhenius plots for the calculated ionic conductivity for $(Ba_xLa_{1-x})InO_{3-0.5x}$ compared with experimental values.

3. Results and discussion

3.1. Lattice constants and ionic conductivities

Fig. 2 shows the calculated lattice constants of $(Ba_xLa_{1-x})InO_{3-0.5x}$ as a function of Ba content, obtained from our experimental results [6]. The lattice constant increases slightly with increasing Ba content, since a Ba ion has a larger ionic radius than a La ion. The calculated lattice parameters of $(Ba_xLa_{1-x})InO_{3-0.5x}$ were 0.19 ~ 0.34% lower than the experimental values, indicating that the interatomic potentials used in this study were reasonably accurate.

The calculated MSDs of each ion are shown in Fig. 3. The MSD for oxide ion increased continuously with time, while the MSDs for the cations remained relatively constant. These results support a scenario in which only oxide ions diffuse in the lattice and that the Ba-doped $LaInO_3$ is the oxide ion conductor, as has been reported in previous reports [5,6].

Fig. 4 shows an Arrhenius plot of the ionic conductivity obtained from eqs (2)–(4), with experimental data in the composition range from $x = 0.4$ to $x = 0.5$, where $(Ba_xLa_{1-x})InO_{3-0.5x}$ is present in the form of a cubic phase [5]. The calculated ionic conductivity for $Ba_{0.4}La_{0.6}InO_{2.8}$ was ~0.3 kS cm^{-1} lower than experimental data reported by Kim et al. [6] for all simulated temperatures. As reported in a previous experimental study [5], the ionic conductivity in our simulation also decreases with increasing Ba content. This supports the conclusion that the current model is effective for estimating oxide ion diffusion in the cubic phase of Ba-doped LaInO3 perovskite. The activation energies for oxygen migration were derived from the slope of the Arrhenius plot and were determined to be 0.84 eV and 0.77 eV for $Ba_{0.4}La_{0.6}InO_{2.8}$ and $Ba_{0.5}La_{0.5}InO_{2.75}$, respectively. The calculated activation energy also decreases with increasing Ba content, as reported in previous experimental studies. Furthermore, the obtained values shows a small deviation of ~±0.05 eV from experimental values.

All of the calculated data for the lattice constant, the ionic conductivity and the activation energy in this study is in reasonable agreement with previously reported experimental data, indicating that our simulation methods can be successfully used to reproduce the realistic diffusion of oxide ions and can be used to examine the mechanism responsible for the conduction of oxide ions in Ba-doped $LaInO_3$ perovskite.

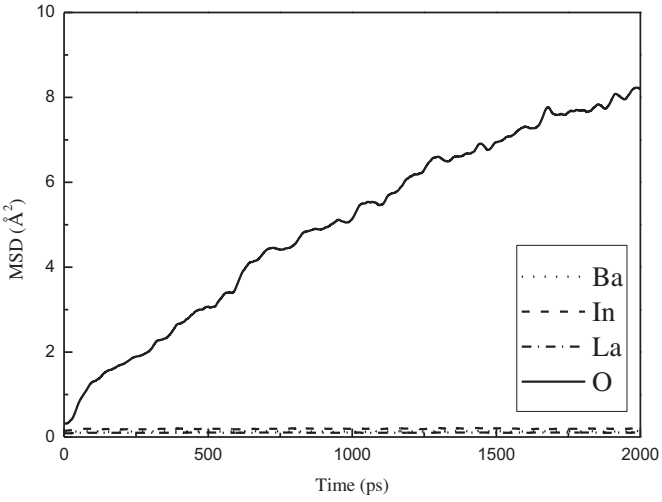

Fig. 3. MSD of ions in $(Ba_{0.4}La_{0.6})InO_{2.8}$ obtained at 900 °C.

3.2. Migration mechanism in the diffusion of oxide ion

Previous studies reported that an increase in Ba content reduced the oxide ion conductivity of Ba-doped $LaInO_3$ in spite of the increase in oxygen vacancies [5,6]. To explain this phenomenon, Kakinuma et al. proposed the concept of a “mobile oxide ion” in which only a limited fraction of the total oxide ions in the lattice are movable and are capable of acting as an effective charge carrier [5]. Kakinuma et al. also calculated the number of mobile oxide ions from experimental data for ion conductivities as a function of La content [5]. Even though the concept of a mobile oxide ion seems to be based on the association effect, it provided only a superficial analysis with macroscopic experimental results, and has not been validated by a theoretical approach. Why can only a fraction of the oxide ions diffuse and act as active mobile charge carriers in Ba-doped $LaInO_3$? To answer this unsolved question, we recorded the trajectories of all oxide ions for some selected calculated results.

In the ABO_3 perovskite structure, the nearest neighbors for each oxide ion consist of four *A*-site cations and two *B*-site cations. Hence, an oxygen octahedron in the perovskite structure could be characterized as having the ionic configuration of an oxygen site

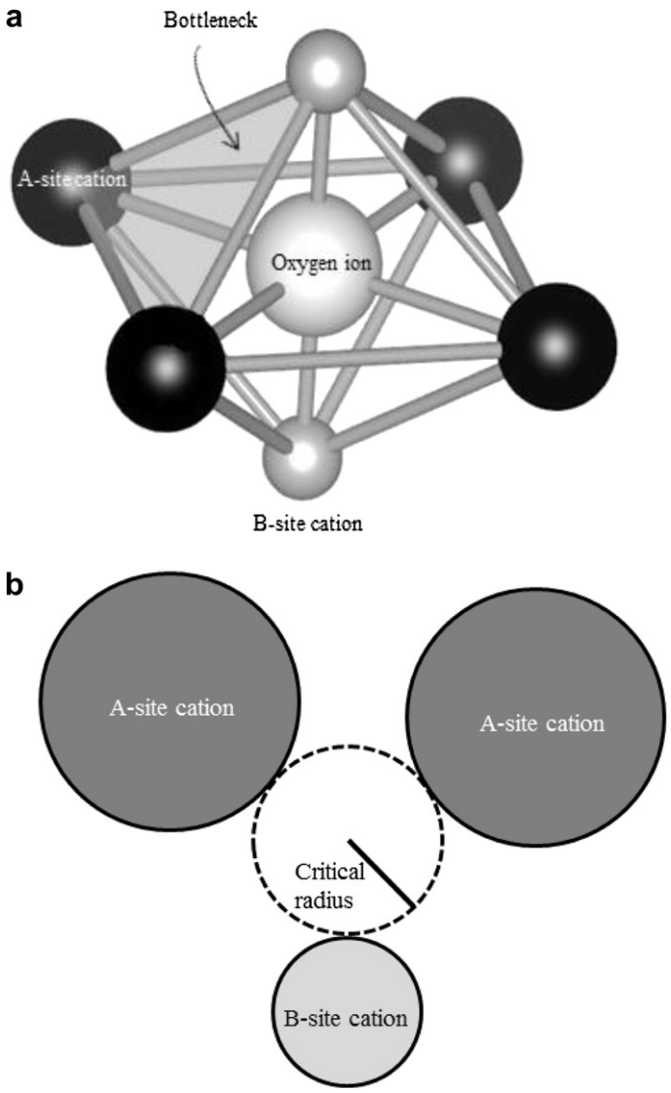

Fig. 5. (a) Oxygen octahedral site in perovskite oxide (b) critical radius at the bottleneck.

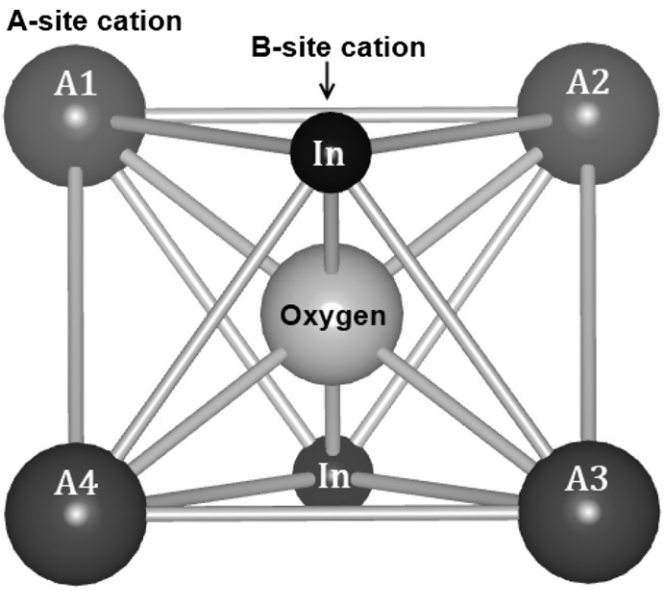

Oxygen-site configuration	Notation (A1A2A3A4)
4-Lanthanum	LaLaLaLa
3-Lanthanum, 1-Barium	LaLaLaBa
2-Lanthanum, 2-Barium (parallel)	LaLaBaBa
2-Lanthanum, 2-Barium (cross)	LaBaLaBa
1-Lanthanum, 3-Barium	LaBaBaBa
4-Barium	BaBaBaBa

Fig. 6. Oxygen sites in the perovskite structure classified according to the order of neighboring *A* site cations.

and its neighboring ions as shown in Fig. 5. For Ba-doped $LaInO_3$, La and Ba are available as *A*-site cations while only In is fixed as a *B*-site cation. Therefore, six species of the oxygen octahedra shown in Fig. 6 can all be present. According to the conventional hopping mechanism, the oxide ions must pass through a bottleneck which points out a so called "saddle point" [8]. The saddle point is mathematically defined as a stationary point on the energy surface between two local minima and two local maxima, while the bottleneck is defined as the point in the structure along the migration path where the space is most constricted. Since this study deals with structural environment of pathway in the oxygen diffusion, we adopt the concept of bottleneck to describe the structural environment about the saddle point.

For the oxygen diffusion in this study, the bottleneck in the pathway is defined as the triangular face shared between adjacent oxygen octahedra and consisting of two *A*-site cations and one *B*-site cation. If we assume that an ion is a rigid sphere [18], the size of each bottleneck could be determined by calculating the critical radius, i.e., the radius of a circle inscribing two *A*-site cations and one *B*-site cation. The critical radius of the bottleneck is determined by the local distribution of the *A*-site cation species, Ba and La ions. For example, in the $La_{0.6}Ba_{0.4}InO_{2.8}$ at 900 °C, the critical radii of the Δ LaLaIn, Δ LaBaIn and Δ BaBaIn bottlenecks were calculated to be 1.072 Å, 0.964 Å and 0.868 Å, respectively. This means that the bottlenecks have small critical radii when a Ba ion is located within it. This also implies that oxide ion conductivity is affected by the local distribution of *A*-site cations.

To determine the effect of the local distribution of *A*-site cations, we prepared 6 configurations notated A, B, C, D, E and F with different local distributions of Ba ions for $La_{0.6}Ba_{0.4}InO_{2.8}$ as represented in Table 2. All of the oxide ion migrations for the 6 selected configurations were analyzed after performing an MD simulation at 900 °C. Successive hops between only two adjacent sites were not counted as the number of ion migrations. Table 3 shows the oxygen migration statistics which was analyzed with the oxygen site pair and the migration pathway. Though the combination of the adjacent oxygen sites is calculated as 6 × 6 species, all of the adjacent oxygen sites pairs share two *A*-sites cations and one *B*-site cation. Hence, some combinations of an oxygen site pair cannot exist. It is possible for an oxide ion in an oxygen site pair to diffuse through different bottlenecks. As a result, 22 types of oxide ion migrations are available in Ba-doped $LaInO_3$. The number of oxygen site pairs, N_p, and the number of oxide ions migrating between the oxygen sites pair, N_m, were obtained as the average values for the 6 configurations with different ionic distributions. The total number of oxygen site pairs, the available number of pathways for oxide ionic diffusion, was counted as 2400, since there were 600 oxygen sites with 8 neighboring adjacent oxygen sites in this simulation. The diffusion frequencies per pair of oxygen sites were characterized with N_m/N_p, which means the number of migrating oxide ions

Table 2
Configurations simulated to study the effect of the local distribution of *A*-site cations.

Site-type	Configuration					
	A	B	C	D	E	F
LaLaLaLa	46	65	73	56	82	61
LaLaLaBa	220	203	197	224	196	213
LaLaBaBa	164	138	150	1128	136	134
LaBaLaBa	102	99	86	104	77	101
LaBaBaBa	64	85	85	80	98	87
BaBaBaBa	4	10	9	8	11	4

per oxygen site pairs. The diffusion frequency per oxygen site pair indicates whether the bottleneck between the oxygen site pairs act as an acceptable diffusion pathway or not. As shown in Table 3, there were some oxygen sites pairs with $N_m/N_p = 0$ as on the case of LaLaBaBa–BaBaBaBa, which indicates that some diffusion pathways are not functional. Furthermore, we classified the oxygen migration by their pathways passing through bottlenecks, and the results are shown in Table 4. While ~90% of the oxide ions passed through the largest bottlenecks, Δ LaLaIn, diffusion through the bottlenecks of Δ LaBaIn is at a level of about 10%. According to the results, Ba comprised 40% of the *A*-site cations but the contribution of Ba cations to oxygen diffusion was no more than ~10%. This result proves that oxide ions have a preference for larger bottlenecks as a pathway to adjacent oxygen sites. No diffusion through the smallest bottlenecks of Δ BaBaIn was found, meaning that Δ BaBaIn functions as an obstacle to the diffusion of oxide ions. The calculation showed that fully immobile oxygen was located exclusively in the BaBaBaBa site, however, oxide ions

Table 3
Oxygen ion migration statistics analyzed with oxygen site pairs and migration pathway.

No.	Oxygen site pair	Bottleneck in the pathway	N_p	N_m	N_m/N_p
1	LaLaLaLa–LaLaLaLa	Δ LaLaIn	77	877	11.4
2	LaLaLaLa–LaLaLaBa	Δ LaLaIn	269	1628	6.1
3	LaLaLaLa–LaLaBaBa	Δ LaLaIn	88	264	3.0
4	LaLaLaBa–LaLaLaBa	Δ LaLaIn	212	780	3.7
5	LaLaLaBa–LaLaLaBa	Δ LaBaIn	141	126	0.9
6	LaLaLaBa–LaLaBaBa	Δ LaLaIn	143	309	2.2
7	LaLaLaBa–LaLaBaBa	Δ LaBaIn	187	49	0.3
8	LaLaLaBa–LaBaLaBa	Δ LaBaIn	254	109	0.4
9	LaLaLaBa–LaBaBaBa	Δ LaBaIn	113	26	0.2
10	LaLaBaBa–LaLaBaBa	Δ LaLaIn	26	32	1.2
11	LaLaBaBa–LaLaBaBa	Δ LaBaIn	66	22	0.3
12	LaLaBaBa–LaLaBaBa	Δ BaBaIn	57	0	0.0
13	LaLaBaBa–LaBaLaBa	Δ LaBaIn	181	31	0.2
14	LaLaBaBa–LaBaBaBa	Δ LaBaIn	67	9	0.1
15	LaLaBaBa–LaBaBaBa	Δ BaBaIn	141	0	0.0
16	LaLaBaBa–BaBaBaBa	Δ BaBaIn	29	0	0.0
17	LaBaLaBa–LaBaLaBa	Δ LaBaIn	110	43	0.4
18	LaBaLaBa–LaBaBaBa	Δ LaBaIn	104	17	0.2
19	LaBaBaBa–LaBaBaBa	Δ LaBaIn	24	2	0.1
20	LaBaBaBa–LaBaBaBa	Δ BaBaIn	82	0	0.0
21	LaBaBaBa–BaBaBaBa	Δ BaBaIn	27	0	0.0
22	BaBaBaBa–BaBaBaBa	Δ BaBaIn	3	0	0.0
Total			2400	4324	

Table 4
Diffusion pathways of oxygen ion characterized with bottleneck in the pathway.

Bottleneck in the pathway	N_m	Pathway selected probability
Δ LaLaIn	3890	90%
Δ LaBaIn	434	10%
Δ BaBaIn	0	0%
Total	4324	100%

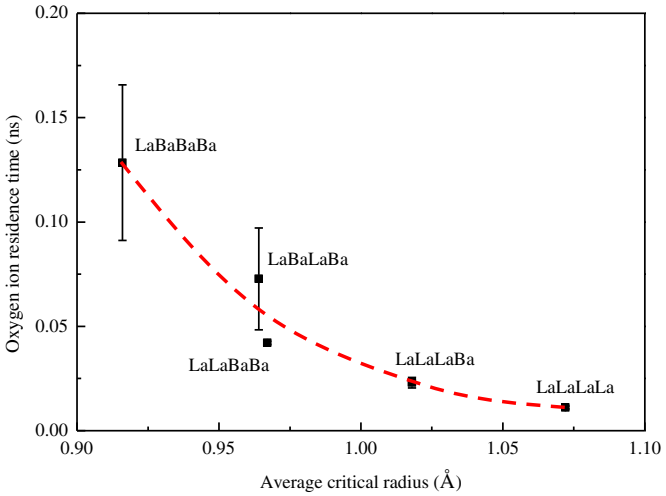

Fig. 7. Oxide ion residence time for $(Ba_{0.4}La_{0.6})InO_{2.8}$ as a function of the average critical radius at 900 °C.

neighboring Ba cations also proved to be difficult to move. These analyses provide fundamental insights into experimental results reported by Kakinuma et al. [5].

We also introduced the concept of the oxide ion residence time to demonstrate how long an oxide ion can remain in an octahedral oxygen site. The oxide ion residence time for the oxygen site was obtained as an average value for all of the equivalent sites. Fig. 7 shows the oxide ion residence time for the oxygen site as a function of the average critical radius of each oxygen site, in which the oxide ion residence time decreases with increasing average critical radius. The oxide ion residence time in the BaBaBaBa site is not shown in Fig. 7 since its oxide ions were immobile. Since the localized La-rich area should contain numerous large bottlenecks, the oxide ions neighboring La cations would easily move, while oxide ions neighboring Ba cations would be more difficult to move. Therefore, it appears that oxide ions diffuse following a La-rich path in Ba-doped $LaInO_3$. Consequently, the use of Ba as a dopant results in the formation of not only oxygen vacancies in the $LaInO_3$ lattice structure, but also bottlenecks with various critical radii, depending on the distribution of Ba ions. Though oxygen vacancies provide electrical charge carriers, the frequency at which oxide ions migrate is strongly dependent on the size of the localized bottlenecks. Bottlenecks that are too small would not permit oxide ions to move to the adjacent site, which means that oxide ions located in localized Ba-rich area would move with difficulty through the Ba-rich bottlenecks. Therefore, it can be concluded that the ionic conductivity of Ba-doped $LaInO_3$ is affected not only by the amount of oxygen vacancies, but also by the distribution of the dopant ions.

4. Conclusions

Oxide ion conduction in the Ba-doped $LaInO_3$ perovskite was successfully reproduced by employing an empirical molecular dynamics simulation technique. These simulation results show that the oxygen vacancies increase with increasing Ba content but oxide ionic conductivity decreases, which is in good agreement with previously published experimental data. The trajectories of each oxide ion were also analyzed with respect to the local ionic configuration of the oxygen octahedral sites. The oxygen migration mechanism in Ba-doped $LaInO_3$ perovskite was successfully analyzed, and the results are consistent with oxide ions diffusion via La-rich areas in the lattice structure. The theoretical analyses of oxygen conduction in Ba-doped LaInO3 reported in this study

indicate that oxygen conduction is affected, not only by the amount of oxide ion vacancies but also by the distribution of doped Ba ions.

References

[1] T. Ishihara, H. Matsuda, Y. Takita, J. Am. Chem. Soc. 116 (1994) 3801.
[2] K.T. Lee, S. Kim, G.D. Kim, H.L. Lee, J. Appl. Electrochem. 31 (2001) 1243.
[3] K. Nomura, T. Takeuchi, S. Tanase, H. Kageyama, K. Tanimoto, Y. Miyazaki, Solid State Ionics 154–155 (2002) 647.
[4] K. Nomura, T. Takeuchi, S.-I. Kamo, H. Kageyama, Y. Miyazaki, Solid State Ionics 175 (2004) 553.
[5] K. Kakinuma, H. Yamamura, H. Haneda, T. Atake, Solid State Ionics 140 (2001) 301.
[6] H.-L. Kim, K.-H. Lee, S. Kim, H.-L. Lee, Jpn. J. Appl. Phys. 45 (2A) (2006) 872.
[7] M. Cherry, M.S. Islam, C.R.A. Catlow, J. Solid State Chem. 118 (1995) 125.
[8] M.S. Islam, M. Cherry, C.R.A. Catlow, J. Solid State Chem. 124 (1996) 230.
[9] M.S. Islam, Solid State Ionics 154–155 (2002) 75.
[10] Y. Yamamura, C. Ihara, S. Kawasaki, H. Sakai, K. Suzuki, S. Takami, M. Kubo, A. Miyamoto, 160 (2003) 93.
[11] C.A.J. Fisher, M. Yoshiya, Y. Iwamoto, J. Ishii, M. Asanuma, K. Yabuta, Solid State Ionics 177 (2007) 3425.
[12] M.P. Tosi, F.G. Fumi, J. Phys. Chem. Solids 25 (1964) 45.
[13] F.G. Fumi, M.P. Tosi, J. Phys. Chem. Solids 25 (1964) 31.
[14] R.A. Buckingham, Proc. R. Soc. Lond. A. 168 (1938) 264.
[15] S.J. Plimpton, J. Comput. Phys. 117 (1995) 1.http://lammps.sandia.gov.
[16] Y. Tamai, Y. Kawamoto, Chem. Phys. Lett. 302 (1999) 15–19.
[17] T. Ishigaki, S. Yamauchi, K. Kishio, J. Mizusak, K. Fueki, J. Solid State Chem. 73 (1988) 179.
[18] R.L. Cook, A.F. Sammells, Solid State Ionics 45 (1991) 311.